EXPERIMENTAL AND NUMERICAL INVESTIGATION OF DRIVING POTENTIAL OF BIOMASS-PELLET HOT AIR GENERATOR FOR COUPLING WITH ABSORPTION HEAT PUMP

by

Marko N. ILIĆ[a], Velimir P. STEFANOVIĆ[a], Dmytro BREGA[b], Dragoljub S. ŽIVKOVIĆ[a], and Saša R. PAVLOVIĆ[a]*

[a] Faculty of Mechanical Engineering, University of Niš, Niš, Serbia
[b] Department of Aerodynamics at National Aerospace,
University Named After H. E. Zhukovsky, Kharkiv, Ukraine

This paper presents a numerical and experimental study of a heating system that consists of hot air generator driven by biomass pellet burner to drive the NH$_3$-water absorption heat pump made by Robur. The aim of this work is to fully test the system of hot air generator for thermal potential, by developing a thermal field, while driving the absorption heat pump of medium capacities for residential purposes, and to make model of predicting the efficiencies of heating comparing to conveyed heat in desorber of absorption heat pump. Numerical simulations of the hot air generator were performed in the commercial software ANSYS FLUENT and CFX. The experimental part was carried out in the laboratory of the Faculty of Mechanical Engineering in Niš, where the temperature and velocity measurements were obtained and compared to numerical results. Results were obtained for mass air-flow through the hot air generator and desorber of 0.17 and 0.2552 kg/s, pellet burner power of 15 kW, 18 kW, 21 kW, 24 kW, 27 kW, and 30 kW, with air inlet temperature in desorber of around 89-140 °C. The heating efficiency of the absorption heat pump goes from 1.01 to 1.37. The heat loss over the surfaces of hot air generator goes from 0.6-0.9 kW depending on ambient air and surface temperatures. The system has the potential to be applied in low temperature heating and the spare heat from combustion products and residual hot air can be used for different purposes.

Key words*: biomass, pellet, hot air generator,
ammonia absorption heat pump, CFD*

Introduction

The increase in energy consumption in the world has an expanding tendency, it is a consequence of the faster technological development of civilization and the living standard of people, such as the need for thermal comfort [1]. Research is currently underway on the efficient utilization of RES, such as, biomass, solar energy, and other forms in absorption technology, in terms of efficiency and applicability. [2].

The building sector is responsible for over 30% of total energy consumption, even higher percentage is present in more developed countries [3]. It is also one of the largest consumers of primary energy and emitters of GHG. Therefore, it is vital that all these energy needs

---

* Corresponding author, e-mail: marko.n.ilic@masfak.ni.ac.rs

3660

Ilić, M. N., *et al.*: Experimental and Numerical Investigation of Driving ...
THERMAL SCIENCE: Year 2023, Vol. 27, No. 5A, pp. 3659-3673

are covered from so-called clean, renewable energy sources [4, 5]. As a result, global warming causes more and more electricity to be consumed for cooling in the summer months, and even that consumption in some parts of the planet exceeds the consumption of electricity for heating in winter [6]. Biomass is one of the most important forms of primary energy belonging to renewable sources, with reduced emissions of pollutants [7]. The advantages of using biomass are that it can always be used regardless of weather conditions and that it is always available in the regions where it is exploited, while the disadvantage is that there are additional costs of conversion, transport and preparation into a suitable form for use, Chambon *et al.* [8].

In addition solar energy, it is one of the forms of renewable energy and represents a potential solution this problem in winter heating and cooling, during warm period of the year, using absorption technology [9]. This technology is promising given that the biomass as a RES will contribute more than 10% of the global power supply [10]. The application of biomass has great prospects, especially in areas where it is generated and where there is a need [11], as it is the case with Serbia. Absorption chillers are systems that use heat in a desorber-generator from an industrial process or from biomass, solar energy, waste heat, for driving the process of cooling or heating. Instead of a compressor, which consumes a significant amount of electricity, desorber is essentially a heat exchanger, where it directly absorbs generated heat at higher rate and efficiency. To start this process, heat of a certain temperature potential is required, which depends on the heat carrier fluid, the mixture of fluids used in the absorption chiller and the working pressure [12]. The advantage of using solar systems in absorption cooling technology is that solar energy is used directly in the absorption process without too many conversions, but the disadvantage is that there is uncertainty in its use because it depends on weather conditions and can be used only when there is sun [13].

The following research shows the efforts of researchers in the exploitation of RES with technology, working medium and temperatures in the vital parts of the absorption chillers to the generator, evaporator, absorber and their achieved efficiencies. Thus, Patela *et al.* [14] examined the effect of the variable operating temperature in the desorber-generator, heat carrier is thermal oil Syltherm800 coming out of the solar field to absorption chiller NH_3-water, where the oil temperature range was from 80-120 °C at the desorber inlet .

Bellos *et al.* [15] performed thermodynamic research on a double-effect absorption chiller with a new working fluid LiCl-water, which is driven by heat from a parbolic trough solar collector via Therminol VP-1 oil, and came to the conclusion that the best exergetic coefficients of COPex utilization occur at lower input temperatures in the desorber from 80-110 °C. She *et al.* [16] tested a two-stage absorption chiller with LiBr-water and LiCl-water in the second stage where the operating heat was at a lower temperature level of about 70 °C at the inlet to the lower pressure desorber and the higher pressure desorber. The overall efficiency was higher than that of a similar two-stage system with a higher operating temperature and only LiBr-water. Moreover, Praham *et al.* [17] proved that lower operating temperatures in the desorber of about 60-70 °C are possible with absorption chillers based on the LiCl-water mixture and that the same efficiency coefficient is achieved as with the LiBr-water system.

In order to improve the efficiency of absorption chillers, they are formed to be multi-stage, but the disadvantage is that in order to work they require a higher inlet temperature in the desorber, over 180 °C, which brings additional burden to the system [18]. At the moment, single-, two-, and three-stage absorption chillers are the most common on the market, most often using a mixture of LiBr-water or NH_3-water as the working medium. The operating temperatures that should enter the desorber-generator of single-stage absorption chillers from the heat

source are between 70-90 °C, and their COP is about 0.65, in two-stage and three-stage chillers the operating temperature is between 180 °C and 240 °C, while the COP utilization coefficient is about 1.4-1.8 [19, 20]

Therefore, multi-stage absorption chillers become interesting due to the higher degree of COP utilization over 1, however, they require significantly higher inlet temperatures to the desorber-generator, which increases the costs of producing high temperature heat sources by over 180 °C, [21, 22]. Xu *et al.* [23] investigated the influence of the inlet temperature in the generator-desorber of the absorption chiller LiBr-water, which comes from the solar field via thermal oil and goes from 95-120 °C, the absorption chiller had the ability to work in one-stage and two-stage modes and change the work simultaneously while performances were examined. The COP utilization coefficient ranged from 0.6-1.08. Rego *et al.* [24] performed testing of hot gases of the exhaust system in an internal combustion car and its temperature potential for the drive of the absorption cooling system in the car, which worked on the basis of NH_3-water. The exhaust gases coming out of the internal combustion engine carry with them part of the heat that remains unused in ordinary cars, in this case contributing to the overall increase in efficiency by transferring heat to the absorption system. Thus, it was observed that the operating temperatures of 180 °C, 200 °C, 240 °C, and 270 °C give different results. The absorption cooling system proved to be unstable at higher temperatures of 240-270°C with low COP due to overheating of the cooling fluid vapor and the lack of possiblity of condensation in the condenser, while the stable operating mode was achieved at 200 °C. The same conclusion was reached in the works of Koehler *et al.* [25] Manzel *et al.* [26]. Cai *et al.* [27] have developed a dynamic model for calculating the thermodynamic quantities of a single-stage absorption chiller. Namely, their numerical calculation with the initial boundary conditions quickly leads to a steady-state of operation of the absorption chiller, and the model very quickly converges to the real parameters and with minor changes in the boundary conditions. It was noticed that the efficiency coefficient of COP increases from 0.55-0.71 when the input operating temperatures in the generator-desorber decrease from 435-344 K.

Pandya *et al.* [28] mathematically performed thermodynamic temperature optimization in the generator-desorber of the LiBr-water absorption chiller, analyzing the minimum temperature in the desorber for the system to function. It has been observed that the minimum operating temperatures of the system in the generator decrease together with the temperature in the evaporator and increase together when the temperature in the condenser increases. When the temperatures in the generator rise from 90-108 °C, the efficiency coefficient COP rises to half of the range of these temperatures and from half retains a constant value, *i.e.*. It grows from 0.2-0.69.

It was noticed [29] that the generator-desorber and its operating temperature and construction, in addition the absorber and evaporator, have the greatest influence on the exergetic coefficient of efficiency of the system and the loss of exergy. It has been shown that as much as 80% of energy loss occurs in the generator-desorber of the absorption chiller due to the mismatch of operating parameters and operating temperature of the desorber, which depends on the construction of the absorption chiller and the working medium [30]. Li *et al.* [31] investigated the influence of the heat load of desorber-generator, two-stage absorption chiller LiBr-water on the degree of efficiency of the air-cooled COP absorption system. It has been noticed that at a lower heat load ratio of the desorber-generator, the efficiency coefficient currently increases. However, it is necessary to determine the optimal heat load ratio of the desorber in order to prevent crystallization in the absorption system.

In the work of Gutierrez-Urueta *et al.* [32] was performed a parametric energy and exergy analysis of the absorption chiller LiBr-water with adiabatic absorber and condenser, where

3662

Ilić, M. N., *et al.*: Experimental and Numerical Investigation of Driving ...
THERMAL SCIENCE: Year 2023, Vol. 27, No. 5A, pp. 3659-3673

it was observed that the exergetic efficiency coefficient depends on the operating temperature in the desorber-generator at a constant temperature of the absorber and condenser. In general, as the temperature in the desorber-generator increases, the exergetic coefficient of efficiency decreases. Therefore, it was calculated that the highest utilization coefficients of cycle I exergy at desorber temperatures are less than 65 °C.

Velasqez *et al.* [33] tested an air-cooled absorption cooling system NH_3-water which is driven by the heat of combustion of natural gas in a desorber-generator of an absorption chiller where part of the heat for desorber operation is regenerated via GAX heat exchangers. They reached the efficiency coefficients of cooling COP_h of 0.86 in summer and heating of 1.86 in winter, at the outlet temperature of the working fluid from the desorber of 200 °C.

Ilić *et al.* [34] simulated temperature profile inside the small pellet stove around 15 kW for possible placement of desorber of single state absorption heat pump. The temperature potential is around 400 °C enough to drive the absorption process. In a subsequent review, Sun [35] compared the thermodynamic states of three different absorption chillers, the first based on NH_3-water, the second NH_3-$LiNO_3$, and the third NH_3-NaSCN. Since all three systems performed the same cooling effect, *i.e.* the power of the evaporator was constant, and the only parameter that influenced the quality of the cooling efficiency coefficient COP_h was the generator-desorber, *i.e.* The amount of heat delivered to the desorber with the temperature level of the driving energy. The NH_3-NaSCN and NH_3-$LiNO_3$ have been observed to be good substitutes for steady-state NH_3-water because they achieve better COP for lower temperatures in the desorber-generator system.

Marcos *et al.* [36], proposed a new way of optimizing COP of cooling of LiBr-water-absorption chillers regardless if it is single or double stage system. In this approach, the model recognizes the condensation temperatures and concentrations of the working mixture with the working temperatures in the desorber-chiller generator of 92.8-57.8 °C. It was observed that the efficiency coefficient for a single-stage system goes from 0.84-0.74, respectively.

Physical and mathematical model of the case

Following the previous description of contemporary absorption heat pump (AHP) technology, it can be seen that the majority of driving heat for the AHP desorber comes from solar, gas or waste heat, but very little or none is produced by the direct combustion of biomass-pellets in the desorber. In this research, conducted in the laboratory of the Faculty of Mechanical Engineering in Niš, Serbia, the performance of a single-stage AHP-NH_3-water-GAHP-AR Robur was tested when driving source is hot air inside the desorber, figs. 1 and 2. Hot air is generated in hot air generator, figs. 3 and 4, and it has a biomass-pellet burner – Pelltech PV30a (up to 30 kW) on one side [37], and on the other three-speed fan Ruck – EM 315 E2M 01, speed range up to 3000 m^3/h [38]. When connected to the AHP due to connection pressure drop the air-flow goes from 675 to 920 m^3/h or 0.17-0.2552 kg/s. This concept, of hot air injection desorber of AHP was approached for the reason of avoiding direct exposure and contamination of desorber exchange surfaces with dirty products of pellet biomass combustion.

In figs. 3 and 4, the basic dimensions and shape of the hot air generator can be seen as well as fluids flow paths. The generator walls are made of boiler steel with performance that can be found in database [39].

The pellet burns in the burner, where flame and hot gases-combustion products heat the air through the walls of the furnace and the plate heat exchanger located inside the upper part of the generator. The flow paths of combustion products and air are shown in red and blue, respectively. Temperatures inside the generator on the side of combustion gaseous products

Ilić, M. N., *et al.*: Experimental and Numerical Investigation of Driving ...
THERMAL SCIENCE: Year 2023, Vol. 27, No. 5A, pp. 3659-3673

3663

Figure 1. Laboratory of MEF Niš with Pellet Silo on the left, absorption heat pump in the middle and hot air generator on the right with pellet burner
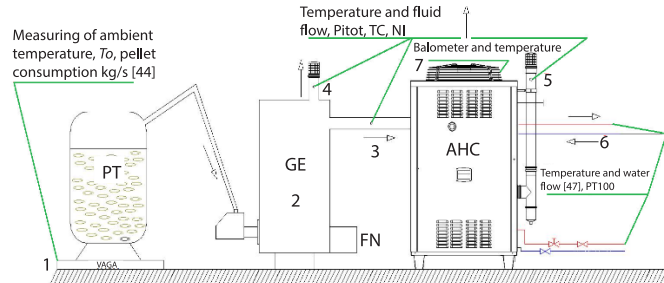
Figure 2. Testing scheme with measurement spots:
1 – pellet consumption measurement [kgs^{-1}], 2 – hot air generator temperature measurement with thermocouples (hereinafter TC) K-type, 3-5 – temperature measurement of hot air and combustion products and fluid-flow with TC K-type and Pitot-Prandtl probe, 6 – water temperature and flow measurement with PT100 probes and Kamstrup flowmeter, and 7 – balometer and TC
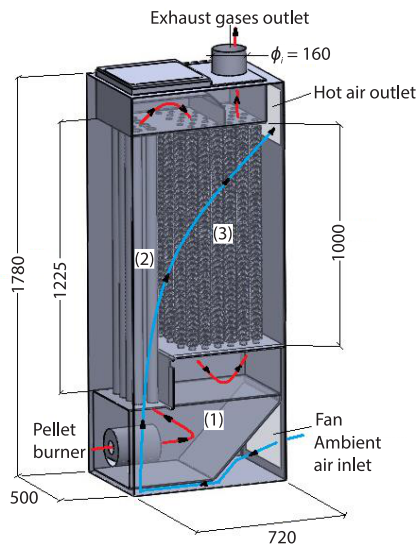
Figure 3. – Basic dimensions in mm and path flows of hot air generator (red-combustion products, blue – air)
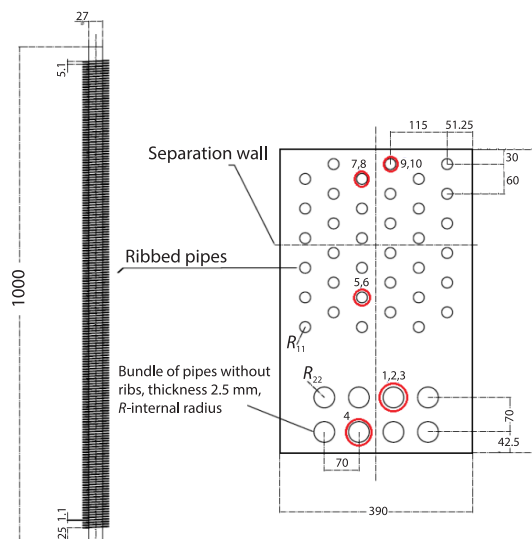
Figure 4. Dimensions of the pipe heat exchanger in mm and thermocouple positions represented numbers (thermocouple 1, 2, 6, 8 are positioned in down part of the pipes 1.8 cm from the edge other are in upper parts)

were measured using the acquisition system LabVIEW with NI cDaQ 9188 chassis [40] and 16 channel NI 9213 module [41] for thermocouples (*K*-type) that were fully calibrated with ±0.5% accuracy and prepared for measurements figs. 5 and 6.

Heat is transferred from hot combustion products to colder air along the entire flow path. The flow of combustion products and hot-air were measured with Testo 400 [42] and Pitot-Prandtl probe $\varnothing_i = 7$ mm, [43], at 10 pipe dimeters from the entrance, figs. 7 and 8. From the air side of the generator, air enters from the environment on the opposite side from the burner (ambient temperature, T_0) and is blown into the lower part of the generator by a fan, where it

encounters the outside hot wall of the burner chamber and floods the chamber. The air continues to flow upwards where it encircles the smooth pipes first and then the front ribbed part and then the back ribbed part of pipe heat exchanger (TC – 10 and TC – 15), measured humidity of hot air was 35-36 %.

Figure 5. Mounted TC in pipe heat exchanger of hot air generator
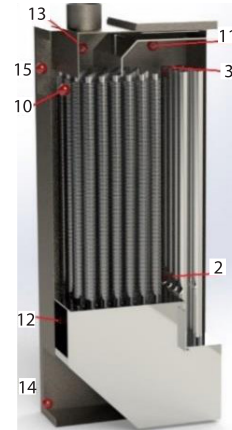
Figure 6. Graphical positions of TC, 15-desorber inlet
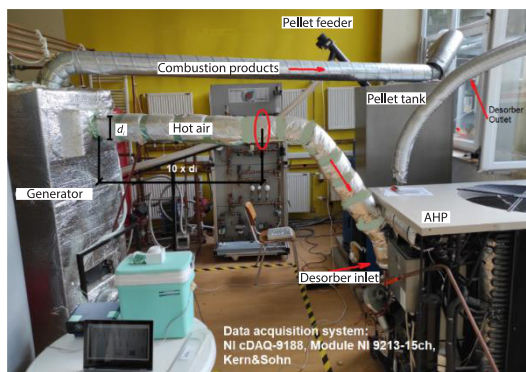
Figure 7. Experimental set-up in laboratory of FMEN
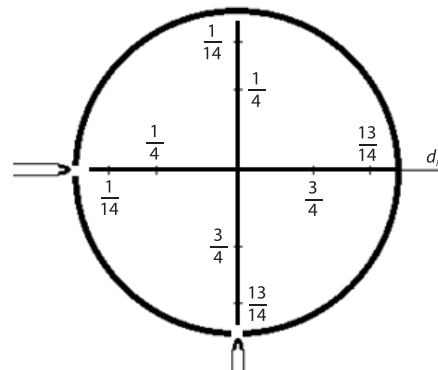
Figure 8. Configuration of volume flow-grid measurement as per EN 12599 in pipes with Pitot – Prandtl probe Ø = 7 mm

Finally, heated air, reaches the outlet in the upper part of the generator above the fan where the outlet air temperature is measured with TC – 15. The outlet diameter of the hot air opening is $Ø_i = d_i = 127$ mm. Hot air then enters the desorber of the AHP and leaves it throught the desorber outlet, where the temperature was measured by TC K-type and Testo 400. On the left side of the generator, there is a pellet tank with weight scale Kern and Sohn – KMB-TM, [44], which continuously supplies the burner with the appropriate amount of pellets in accordance with the set power on the burner and the operating mode of the generator. The characteristic temperature measuring points on the hot combustion products side and on the air side are shown in fig. 8 in accordance to EN 12599 and error ±2.5%. The entire generator is lined

with 10 cm of mineral wool insulation [45] and over reflective air aluminum foil with bubble thickness of 2.5 mm with its thermophysical characteristics found in [46] to reduce heat losses to the lowest possible level. The total resistance coefficient of passage through the generator wall, insulation layers and aluminum air foil is 3.2 m^2K/W. Heating capacity on the water side of the AHP was measured by Kamstrup multical 402 calorimeter [47] and two PT – 100 probes on outlet and inlet pipes, with measured water flow of 2.5 m^3 per hour ±1.5%.

Numerical model of hot air generator and
COP determination of AHP

Mathematical models consist of two parts, first part is numerical simulation of the hot air generator and its performances to validate it with real measurements, and the second part is calculating heating efficiencies of AHP by acquired measured parameters.

Firstly, the numerical simulation of biomass hot air generator was performed with both steady and transient analysis. First steady analysis was carried to reach a certain level for residuals, after convergence criteria has reached 10^{-3} for scalar and 10^{-6} for energy residuals, transient settings were applied. Calculation time per case took around two days on computer i7-5700HQ CPU at max 3.50 GHz with 2.70 GHz processor and 32 GB of RAM.

Considering the complicated nature of modeled system, following boundary conditions and assumptions were used:
– Only a half of geometry was considered.
– Reynolds decomposition is used to simplify Navier-Stokes equations.
– A burner was simulated using a heat source.
– A mixture of air and CO_2 was used in simulation.
– A real geometry for a heat exchanger was simplified using porosity model.
– From the side of exhaust gases, the velocity inlet and pressure outlet were set up where ambient pressure was set to 0 Pa.
– From the side of hot air, the mass inlet and mass outlet were defined.
– No-slip condition is applied to all walls.

A commercial code ANSYS FLUENT was used for numerical simulations.

The geometry as well as the mesh was created via Workbench platform, figs. 9 and 10, a model was created according to the dimensions of the experimental set-up.
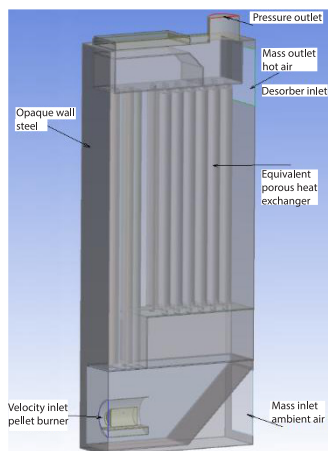
Figure 9. Computational domain of the case   **Figure 10. Tetrahedral mesh of the domain**
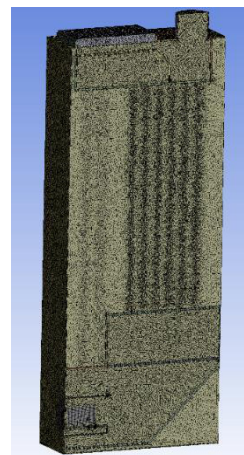
3666

Ilić, M. N., *et al.*: Experimental and Numerical Investigation of Driving ...
THERMAL SCIENCE: Year 2023, Vol. 27, No. 5A, pp. 3659-3673

The mesh size was chosen according to expected velocities magnitude. Several simulations were done to check case sensitivity on a mesh size and to obtain a discretization error using a grid convergence index, tab. 1. It was found that the difference in temperature value on outlet boundary condition between fine and medium mesh is less than 1%. Initially a mesh with half a million of elements was used, however after mesh dependency check, it was found that 1 million of cells is enough to obtain an accurate solution with the minimum computational time.

Table 1. Mesh size of the domain

Mesh size	Coarse	Medium	Fine
Number of elements	7278021	10405293	14436821
Number of nodes	3611401	4690774	5929862

The combustion of gases is governed by a set of equations describing the conservation of mass, momentum, energy, and species. Excluding the mass forces, baro – and thermal diffusion, the equations are:

$$\frac{\partial \rho}{\partial t} + \nabla(\rho \mathbf{u}) = 0 \tag{1}$$

$$\frac{\partial(\rho \mathbf{u})}{\partial t} + \nabla(\rho \mathbf{u}\mathbf{u}) = -\nabla P + \nabla \tau_{\text{eff}} \tag{2}$$

$$\frac{\partial(\rho h)}{\partial t} + \nabla(\mathbf{u}\rho h) = \frac{\partial P}{\partial t} + \mathbf{u}\nabla P +$$

$$+\nabla\left(\lambda_{\text{eff}}\nabla T - \sum_i h_i J_i + \tau_{\text{eff}}\mathbf{u} \right) + \sum_{i=1}^{N} Q^i - Q_{\text{rad}} \tag{3}$$

$$\frac{\partial(\rho \mathbf{u})}{\partial t} + \nabla(\rho \mathbf{u}\mathbf{u}) = -\nabla P + \nabla \tau_{\text{eff}} \tag{4}$$

where ρ [kgm^{-3}] is the density, $\mathbf{u}$ – the velocity vector, t [second] – the time, and P [Pa] – the pressure

$$\tau_{\text{eff}} = (\mu + \mu_t)\left(\nabla\mathbf{u} + (\nabla\mathbf{u})^T - \frac{2}{3}I(\nabla\mathbf{u}) \right)$$

is the effective stress tensor (*i.e.*, the sum of the viscous and turbulent stresses), μ [Pa·s] – the viscosity, μ_t – the turbulent viscosity, I – the unit tensor, h [J] – the enthalpy of the mixture, $\lambda_{\text{eff}} = \lambda + \lambda_t$ – the effective thermal conductivity, λ [Wm^{-1}K^{-1}] – the laminar heat conductivity, $\lambda_t = C_p\mu_t\text{Pr}_t^{-1}$– the turbulent heat conductivity, C_p [JK^{-1}] – the specific heat, Pr_t – the turbulent Prandtl number, and T [K] – the temperature, [K].

$$h_i = \int_{T_{\text{ref}}}^{T} C_{p,i}\,\mathrm{d}T$$

where $T_{\text{ref}} = 298.15$ K, is the enthalpy of species i, J_i – the diffusion rate vector of species i, $Q^i = h_i^0 R_i/M_i$ [J] – the heat source, Q_{rad} [J] – the radiation heat, Y_i – the mass fraction of species i, D_i [m^{2}s^{-1}] – the diffusion coefficient of species i in the mixture, Sc_t – the turbulent Schmidt number, and R_i – the rate of production of species, i, by chemical reaction.

For current study SST turbulence model was used, which shows good results simulating the wall surface flows. According to this model the turbulent viscosity is calculated:

Ilić, M. N., *et al.*: Experimental and Numerical Investigation of Driving ...
THERMAL SCIENCE: Year 2023, Vol. 27, No. 5A, pp. 3659-3673

3667

$$\mu_T = \frac{0.31 \rho k}{\max\left(0.31\omega; \Omega F_2\right)} \tag{5}$$

where function $F_2 = \tanh(\text{arg}_2^2)$

$$\text{arg}_2 = \max\left(2\frac{\sqrt{k}}{0.09\omega y}; \frac{500\nu}{y^2\omega}\right)$$

is the equals one for the boundary-layer, and equals zero for the free layer, $\Omega = \partial u/\partial n$ – the derivative of the flow rate on the normal to the wall, and k and ω are the turbulence kinetic energy and the specific dissipation rate, respectively.

Parameters k and ω were obtained from the transport equations:

$$\frac{\partial \rho k}{\partial t} + \frac{\partial}{\partial x_i}\left(\rho v_i k\right) = \tau_{ij}\frac{\partial v_i}{\partial x_j} - \beta^*\rho\omega k + \frac{\partial}{\partial x_i}\left[\left(\mu + \sigma_k \mu_t\right)\frac{\partial k}{\partial x_i}\right] \tag{6}$$

$$\frac{\partial \rho \omega}{\partial t} + \frac{\partial}{\partial x_i}\left(\rho v_j \omega\right) = \frac{\gamma}{\nu_\tau}\tau_{ij}\frac{\partial v_i}{\partial x_j} - \beta\rho\omega^2 +$$

$$+ \frac{\partial}{\partial x_i}\left[\left(\mu + \sigma_\omega \mu_t\right)\frac{\partial \omega}{\partial x_i}\right] + 2\rho(1 - F_1)\sigma_{\omega^2}\frac{1}{\omega}\frac{\partial k}{\partial x_j}\frac{\partial \omega}{\partial_j} \tag{7}$$

where

$$\nu_\tau = \frac{a_1 k}{\max\left(a_1\omega; \dfrac{\partial u}{\partial y F_2}\right)}$$

model constant $\Phi_{\text{SST}}(\gamma, \sigma_k, \sigma_\omega, \beta, \beta^*)$ associated with k-ω model constants $\Phi_{k\omega}$ and transformed k-ε model $\Phi_{k\varepsilon}$ as: $\Phi_{\text{SST}} = \Phi_{k\varepsilon} F_1 + (1 - F_1) \Phi_{k\varepsilon}$, $F_1 = \tanh(\text{arg}_1^4)$:

$$\text{arg}_1 = \min\left[\max\left(\frac{\sqrt{k}}{0.09\omega y}; \frac{500\nu}{y^2\omega}\right); \frac{4\rho\sigma_{\omega^2}k}{CD_{k\omega}y^2}\right]$$

and y [m] – the distance to the nearest wall.

To save computational time a real geometry of a heat exchanger was changed to equivalent porous domain, fig. 11, with calculated parameters given in tab. 2.

Table 2. Porosity model settings

Volume porosity	Interfacial area density	Heat transfer coefficient	Area porosity
0.785	413.5 1/m	250 W/m²K	Isotropic

Figure 11. Real geometry of a heat exchanger inside hot air generator and a porous geometry with equivalent characteristics

Several cases were considered using different values for power of a burner and air mass-flow rate according to fan specification, all data are collected in a tab. 3.

3668

Ilić, M. N., *et al.*: Experimental and Numerical Investigation of Driving ...
THERMAL SCIENCE: Year 2023, Vol. 27, No. 5A, pp. 3659-3673

Table 3. Boundary data

	Case 1	Case 2	Case 3	Case 4
Fan air mass-flow rate*	0.2552 kg/s 0.17 kg/s	0.2552 kg/s 0.17 kg/s	0.2552 kg/s 0.17 kg/s	0.2552 kg/s 0.17 kg/s
Power	15 kW	21 kW	24 kW	30 kW
Outside temperature*	25 °C 20 °C	25 °C 20 °C	25 °C 20 °C	25 °C 20 °C
CO_2 mass fraction on burner inlet	0.5	0.5	0.5	0.5

* For each value of power, two cases were considered with different mass-flow rate and outdoor temperature.

For a comparison analysis with experimental data a Sensor TC positions were specified for monitoring the temperature as in real measurement, their co-ordinates are given in tab. 4.

Table 4. Sensor TC positions

Nimber	X [m]	Y [m]	Z [m]
Sensor TC 1	0.05	1.575	0.155
Sensor TC 2	0.07	1.57	0.155
Sensor TC 11	0.01	1.7	0.25
Sensor TC 12	0.01	0.475	0.45
Sensor TC 13	0.01	1.7	0.575
Sensor TC 14	0.17	0.06	0.71
Sensor TC 15	0.17	1.6	0.71

Second part of mathematical model is calculating heating capacity and COP of AHP by acquired real measurement data of heat delivered in desorber by hot air and of heating water. The heat delivered by water side is actually equal to heat gained through the absorber and condenser of AHP:

$$Q_H = Q_a + Q_c = m_w c_w (t_{out} - t_{in}) \tag{8}$$

where Q_H [kW] is the heating power of AHP, Q_a [kW] – the extracted heat from the absorber, Q_c [kW] – the extracted heat from the condenser of AHP, m_w [kgs^{-1}] – the water mass-flow, c_w – the specific heat capacity of water 4.186 kJ/kgK, t_{ou} [K] – the water outlet temperature from AHP, and t_{in} [K] – the water inlet temperature in AHP [K]:

$$Q_D = m_a c_{p,a} (t_{15} - t_{a,out}) \tag{9}$$

where Q_D [kW] is the desorber power of AHP, m_a [kgs^{-1}] – the air mass-flow through desorber of AHP, $c_{p,a}$ [Jkg^{-1}K^{-1}] – the pecific heat capacity of air calc ulated by eq. (10), t_{15} [K] – the averaged air outlet temperature from hot air generator to desorber inlet, and $t_{a,out}$ [K] – the averaged air outlet temperature from AHP desorber.

Thermo physical properties of air were calculated by the following polynomial equation where coeficiencts are defined by table found in [48]:

$$\frac{c_{p,a}}{\rho_a} = A + BT + CT^2 + DT^3 + ET^4 + FT^5 \quad 280 \leq T \leq 550 \tag{10}$$

Table 5. Coefficients of polynomial equations for calculating the density and specific heat capacity of air

	A	B	C	D	E	F
ρ_a	5.4894	$-3.5035 \cdot 10^{-02}$	$1.1762 \cdot 10^{-04}$	$-2.1926 \cdot 10^{-07}$	$2.1534 \cdot 10^{-10}$	$-8.7095 \cdot 10^{-14}$
$c_{p,a}$	9.4431E-01	$8.8556 \cdot 10^{-04}$	$-4.9308 \cdot 10^{-06}$	$1.2709 \cdot 10^{-08}$	$-1.4674E \cdot 10^{-11}$	$6.5316 \cdot 10^{-15}$

Ilić, M. N., *et al.*: Experimental and Numerical Investigation of Driving ...
THERMAL SCIENCE: Year 2023, Vol. 27, No. 5A, pp. 3659-3673

3669

After measurement and calculation of powers with thermophysical properties, the efficiency of the AHP due to desorber air inlet temperature was defined and presented as ratio between water heating capacity and heat gain in desorber:

$$COP_H = \frac{Q_H}{Q_D} \tag{11}$$

Numerical and calculation results

Figures 12-15 represents a numerical and measurement results for a fully converged solution with a given mesh and computational domain for the hot air generator.

Temperature profile of combustion products can be seen on figs. 12-15, for 15 kW and 21 kW of burner power at 0.17 kg/s of mass air-flow and 24 kW and 30 kW of burner power at 0.2552 kg/s of air-flow, respectively. The subsequent figures present the temperature field of combustion gases at 0.2552 kg/s and 24 kW and 30 kW of burner power.
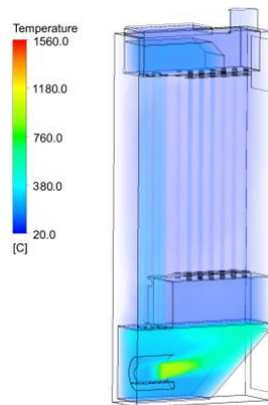
Figure 12. Temperature of combustion products at 15 kW and 0.17 kg/s air-flow
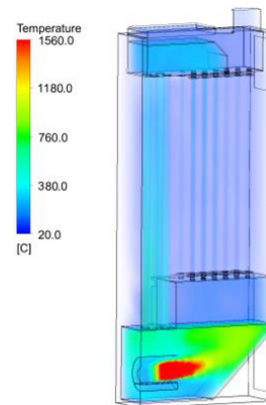
Figure 13. Temperature of combustion products at 21 kW and 0.17 kg/s air-flow
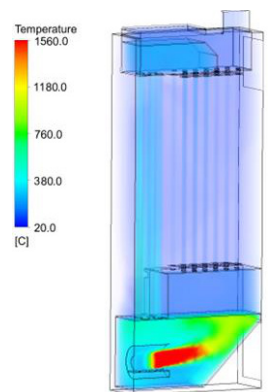
Figure 14. Temperature of combustion products at 24 kW and 0.2552 kg/s of air-flow
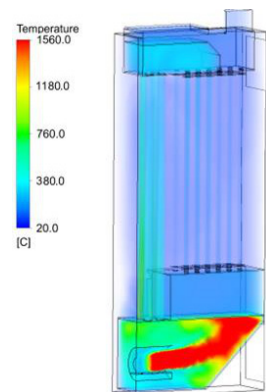
Figure 15. Temperature of combustion products at 30 kW and 0.2552 kg/s of air-flow

3670

Ilić, M. N., *et al.*: Experimental and Numerical Investigation of Driving ...
THERMAL SCIENCE: Year 2023, Vol. 27, No. 5A, pp. 3659-3673

Heat losses over the surfaces of hot air generator due to natural-convection and radiation goes from 0.6-0.85 kW for the range of ambient temperature from 0-8 °C. Surrounding wall surface temperature is in range from 12-16 °C and average temperature of hot air generator is 32-36 °C, as calculated in [49].

In the next diagrams figs. 16 and 17 presented are the real measurements compared to the numerical simulation of temperatures of hot air generator at pellet burner power of 21 kW and air-flow of 0.17 kg/s as validation of numerical simulation. At this power it can be seen that desorber calculated inlet temperature of hot air reaches 115.4 °C while the measured temperature is 116.2 °C.
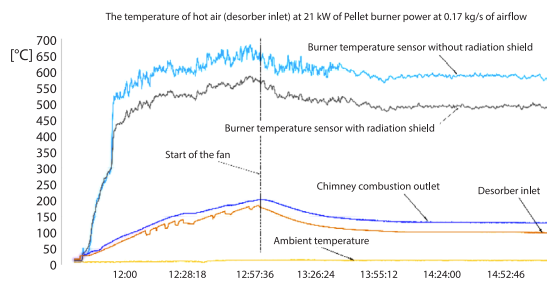
Figure 16. Measured temperatures from the hot air generator at 21 kW burner power and 0.17 kg/s air-flow
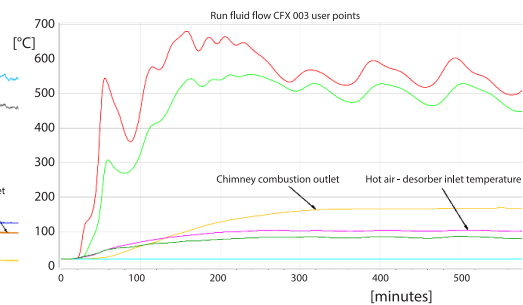
Figure 17. The CFX simulation of hot air generator temperatures at 21 kW burner power and 0.17 kg/s air-flow

After a series of simulations and measurements, the following images figs. 18 and 19 show the average temperatures in the desorber for different burner powers at ambient temperature of 7.5 °C. Numerical simulations are shown with dashed lines, and measurement results are shown with triangles. Given the scale, the averaged deviations of the measured temperatures from the numerical temperatures are not greater than ±4.5 °C.
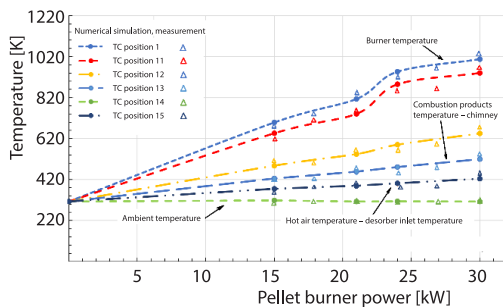
Figure 18. Average desorber inlet temperature TC – 15 and other sensor TC position at 0.17 kg/s air-flow and different burner powers
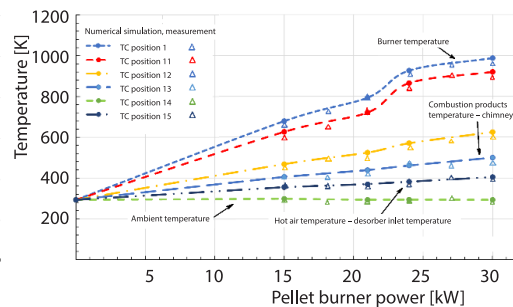
Figure 19. Average desorber inlet temperature TC – 15 and other sensor TC position at 0.2552 kg/s air-flow and different burner powers

The next iteration was determining the efficiency COP of the absorption heat pump depending on the air temperature in the desorber at different burner powers, at air-flows of 0.17 kg/s and 0.2552 kg/s. The efficiency is determined in accordance with the equation eq. (11), and the results are shown in figures figs. 20 and 21.

Ilić, M. N., *et al.*: Experimental and Numerical Investigation of Driving ...
THERMAL SCIENCE: Year 2023, Vol. 27, No. 5A, pp. 3659-3673

3671
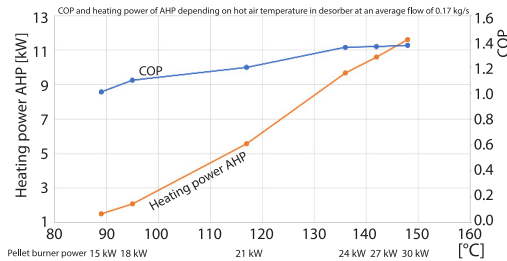
Figure 20. Desorber driving inlet temperature influence on COP of AHP at air-flow of 0.17 kg/s
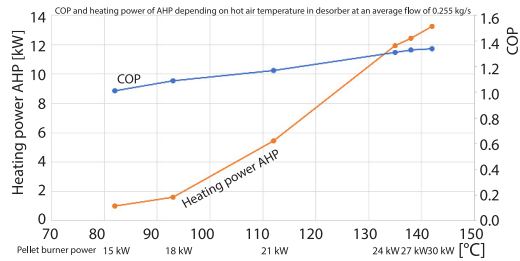
Figure 21. Desorber driving inlet temperature influence on COP of AHP at air-flow of 0.2552 kg/s

It can be seen that the effect of decreasing driving source temperature results in decreasing the COP of AHP and heating capacity, while outlet temperature of heating water goes from 35-31 °C. It is the consenqence of decreased temperature difference in desorber which lowers generation of ammonia refrigerant. Furthermore, reduced quantity of generated refrigerant in desorber, decreases condensation and absorption temperature, while increasing the temperature of evaporation. This process leads to decreasing the COP together with heating capacity of AHP as showed on previous figures. Declinement of COP from around 140-136 °C is slight, around 1.37 and gets lower with further decrease of driving air temperature in desorber to 1.01 for both air-flows.

Fitting curve for COP in relation the temperature in the desorber:

$$COP = -4.346t^3 + 0.016184t^2 - 1.797t + 63.384 \qquad (12)$$

Herold, *et al.*, [50] concluded that COP maintans stable value of 1.5 for the temperature range between 120-150 °C of driving source in desorber, and that further increas in driving source temperature can only increase the heating capacity but not the COP. Achieved COP in this work fits in the concluded range of Herold at all as it is achieved COP of 1.37 at around 150 °C.

Conclusions

Absorption heat pump systems with eco-friendly refrigerants such as NH_3-water represent the alternative for compression heat pump systems with restricted chlorofluorocarbon refrigerants. Absorption systems can make considerable savings in emissions of CO_2 and NO_x gases and reduction of electricity consumption for heating and cooling.

In this research, the aim was to construct and investigate system for heating based on single stage absorption heat pump Robur GAHP-AR and to drive it by hot air that is generated in hot air generator by primary energy of pellets (biomass) in burner. Air-flow to desorber of AHP goes from 0.17-0.2552 kg/s and as driving power of pellet burner increases from 15-30 kW also increases the air temperature inlet from 89-140 °C**.** At higher air desorber inlet temperatures from 136 to around 140 °C the COP of AHP does not vary too much and is around 1.37, while heating capacity is around 11.11-13.2 kW with outlet water temperature of 35 °C. As desorber air inlet temperature decreases also decreases the heating capacity of AHP and COP. Heat losses over the system wall surfaces to surroundings goes within 0.6-0.9 kW. While air outlet from the desorber is at temperatures around 80 °C and air-flows of 0.17-0.2552 kg/s which also has potential for further exploitation for heating some large spaces or utilization in industrial processes. The combustion products leave the system at temperatures of 180-220 °C depending on pellet burner power and air-flow. They also have the capacity to extract heat for

3672

Ilić, M. N., *et al.*: Experimental and Numerical Investigation of Driving ...
THERMAL SCIENCE: Year 2023, Vol. 27, No. 5A, pp. 3659-3673

some heating purposes via some heat recovery equipment in order to bypass contamination from combustion dirts. All in all, it can be said that the goal of constructing and investigating air driven AHP with biomass-driven generator for low temperature heating capacities has been achieved. As a result, the further improvement and optimization of the concept can be carried out, in direction of immediate utilization of heat from biomass combustion in desorber of AHP.

Acknowledgment

References

[1] Wu, X. D., *et al.*, Energy Use in World Economy from Household-Consumption-Based Perspective, *Energy Policy*, *127* (2019), Apr., pp. 287-29

[2] Zhai, X. Q., *et al.*, A Review for Research and New Design Options of Solar Absorption Cooling Systems, *Renewable and Sustainable Energy Reviews*, *15* (2011), 9, pp. 4416-4423

[3] ***. International Energy Agency, Energy Technology Perspectives 2020, https://www.iea.org/reports/energy-technology-perspectives-2020, 2022

[4] Geng, Y., *et al.*, A Bibliometric Review: Energy Consumption and Greenhouse Gas Emissions in the Residential Sector, *Journal of Cleaner Production*, *159* (2017), Aug., pp. 301-316

[5] Zhong, X., *et al.*, The Evolution and Future Perspectives of Energy Intensity in The Global Building Sector 1971-2060, *Journal of Cleaner Production*, *305* (2021), 127098

[6] Clarke, L., *et al.*, Effects of Long-Term Climate Change on Global Building Energy Expenditures, *Energy Economics*, *72* (2018), May, pp. 667-677

[7] Demirbas, M. F., *et al.*, Potential Contribution of Biomass to the Sustainable Energy Development, *Energy Conversion and Management*, *50* (2009), 7, pp. 1746-1760

[8] Chambon, C. L., *et al.*, Techno-Economic Assessment of Biomass Gasification-Based Mini-Grids for Productive Energy Applications: The Case Of Rural India, *Renewable Energy*, *154* (2020), July, pp. 432-444

[9] Behzadi. A., *et al.*, Multiobjective Design Optimization of a Solar Based System for Electricity, Cooling, and Hydrogen Production, *Energy*, *169* (2019), Feb., pp. 696-709

[10] Cao, Y., *et al.*, Waste Heat from a Biomass Fueled Gas Turbine for Power Generation Via an Orc or Compressor Inlet Cooling Via an Absorption Refrigeration Cycle a Thermoeconomic Comparison, *Applied Thermal Engineering*, *182* (2020), 116117

[11] Stolarski, M. J., *et al.*, Bioenergy Technologies and Biomass Potential Vary in Northern European Countries, *Renewable and Sustainable Energy Reviews*, *133* (2020), 110238

[12] Bosnjakovic F., *Technical Thermodynamics*, Holt Rinehart and Winston, Austin, Tex., USA, 1965

[13] Bataineh, K., Taamneh, Y., Review and Recent Improvements of Solar Sorption Cooling Systems, *Energy and Buildings*, *128* (2016), pp. 22-37

[14] Petela, K., *et al.*, Advantages of Variable Driving Temperature In Solar Absorption Chiller, *Renewable Energy*, *114* (2017), Part B, pp. 716-724

[15] Bellos, E., *et al.*, Thermodynamic Investigation of LiCl-H_2O Working Pair in a Double Effect Absorption Chiller Driven by Parabolic trough Collectors, *Thermal Science and Engineering Progress*, *3* (2017), Sept., pp. 75-87

[16] She, X., *et a*l., A Novel Low-Grade Heat-Driven Absorption Refrigeration System With Licl-H_2O and Libr-H_2O Working Pairs, *International Journal of Refrigeration*, *58* (2015), Oct., pp. 219-234

[17] Parham, K., *et al.*, Evaluation and Optimization of Single Stage Absorption Chiller Using (LiCl + H_2O) as the Working Pair, *Advances in Mechanical Engineering*, *5* (2013), pp. 23-31

[18] Gomri, R., Investigation of the Potential of Application of Single Effect and Multiple Effect Absorption Cooling Systems, *Energy Conversion and Management*, *51* (2010), 8, pp. 1629-1636

[19] Shirazi, A., *et al.*, A Systematic Parametric Study and Feasibility Assessment of Solar-Assisted Single-Effect, Double-Effect, and Triple-Effect Absorption Chillers for Heating and Cooling Applications, *Energy Conversion and Management*, *114* (2016), Apr., pp. 258-277

[20] Zhai, X. Q., *et al.*, A Review for Research and New Design Options of Solar Absorption Cooling Systems, *Renewable and Sustainable Energy Reviews*, *15* (2011), 9, pp. 4416-4423

Ilić, M. N., *et al.*: Experimental and Numerical Investigation of Driving ...
THERMAL SCIENCE: Year 2023, Vol. 27, No. 5A, pp. 3659-3673

3673

[21] Ayadi, O., *et al.*, Solar Cooling Systems Utilizing Concentrating Solar Collectors – An Overview, *Energy Procedia*, *30* (2012), pp. 875-883

[22] Liu, Y. L., Wang, R. Z., Performance Prediction of a Solar/Gas Driving Double Effect Libr-H$_2$O Absorption System, *Renewable Energy*, *29* (2004), 10, pp. 1677-1695

[23] Xu, Z. Y., *et al.*, Experimental Evaluation of a Variable Effect Libr-Water Absorption Chiller Designed for High-Efficient Solar Cooling System, *International Journal of Refrigeration*, *59* (2015), Nov., pp. 135-143

[24] Rego, A. T., *et al.*, Automotive Exhaust Gas-Flow Control for an Ammoniae Water Absorption Refrigeration System, *Applied Thermal Engineering*, *64* (2014), 1-2, pp. 101-107

[25] Koehler, J., *et al.*, Absorption Refrigeration System for Mobile Applications Utilizing Exhaust Gases, *Heat and Mass Transfer*, *32* (1997), 5, pp. 333-340

[26] Manzela, A., *et al.*, Using Engine Exhaust Gasas Energy Source for an Absorption Refrigeration System, *Applied Energy*, *87* (2010), 4, pp. 1141-1148

[27] Cai, W., *et al.*, Dynamic Simulation of an Ammonia-Water Absorption Refrigeration System, *Industrial and Engineering Chemistry Research*, *51* (2011), 4, pp. 2070-2076

[28] Pandya, B., *et al.*, Thermodynamic Evaluation of Generator Temperature in LiBr-Water Absorption System for Optimal Performance, *Energy Procedia*, *109* (2017), Mar., pp. 270-278

[29] Aprhornratana, S., *et al.*, Thermodynamic Analysis of Absorption Refrigeration Cycles Using the Second Law of Thermodynamics Method, *International Journal of Refrigeration*, *18* (1995), 4, pp. 244-252

[30] Talbi, M. M., *et al.*, Exergy Analysis: An Absorption Refrigerator Using Lithium Bromide and Water as the Working Fluids, *Applied Thermal Engineering*, *20* (2000), 7, pp. 619-630

[31] Li, Z., *et al.*, Appropriate Heat Load Ratio of Generator for Different Types of Air Cooled Lithium Bromide-Water Double Effect Absorption Chiller, *Energy Conversion and Management*, *99* (2015), July, pp. 264-273

[32] Gutierrez-Urueta, G., *et al.*, Energy and Exergy Analysis of Water-Libr Absorption Systems with Adiabatic Absorbers for Heating and Cooling, *Energy Procedia*, *57* (2014), Dec., pp. 2676-2685

[33] Velazquez, N., *et al.*, Methodology for the Energy Analysis of an Air Cooled Gax Absorption Heat Pump Operated by Natural Gas and Solar Energy, *Applied Thermal Engineering*, *22* (2002), 10, pp. 1089-1103

[34] Ilić, M. N., *et al.*, The CFD Analysis of Temperature Field in Pellet Stove as a Generator of an Absorption Heat Pump, Facta Universitatis Series, *Working and Living Environmental Protection*, *17* (2020), 3, pp. 163-174

[35] Sun, D. W., Comparison of the performances of NH$_3$-H$_2$O, NH$_3$-LiNO$_3$ and NH3-NaSCN absorption refrigeration systems, Da-Wen Sun, *Energy Conversion and Management*, *39* (1998), 5-6, pp. 357-368

[36] Marcos, D. J., *et al.*, New Method for COP Optimization in Water- and air-Cooled Single and Double Effect LiBr Water Absorption Machines, *International Journal of Refrigeration*, *34* (2011), 6, pp. 1348-1359

[37] ***, https://cerbos.ee/img/cms/poletid/pelltech-pellet-burner-PV20a-PV30a-user-manual.pdf

[38] ***, https://www.ruck.eu/ventilatoren/rohrventilatoren1/rohrventilatoren-ac-motor/m-m/130677-em-315-e2m-01?productFrequency=50&filterFrequency=50

[39] ***, https://matmatch.com/materials/minfm33409-en-10028-2-grade-p265gh-normalized-or-normalized-formed-n-

[40] ***, https://www.ni.com/en-rs/support/model.cdaq-9188.html

[41] ***, https://www.ni.com/en-rs/support/model.ni-9213.html

[42] ***, https://www.testo.com/en-TH/testo-400/p/0560-0400

[43] ***, https://www.testo.com/en-IN/pitot-tube/p/0635-2145

[44] ***, http://www.kern-sohn.com/manuals/files/English/KMB_KMS_KMT-BA-e-0720.pdf

[45] ***, https://pim.knaufinsulation.com/files/download/14_fkd-s_thermal.pdf

[46] ***, http://www.star-newmaterial.com/thermal-insulation-material/bubble-foil-insulation/reflective-aluminum-foil-bubble-wrap.html

[47] ***, https://www.kamstrup.com/en-en/cooling-solutions/meters-and-devices/discontinued-products/multical-402

[48] Joseph, H., *et al.*, *Tables of Thermal Properties of Gases*, US Department of Commerce, Washington D.C, USA, 1955

[49] Cengel, Y. A., *Heat Transfer: A Practical Approach*, Mcgraw-Hill, New York, USA, 2002

[50] Herold, K. E., *et al.*, *Absorption Chillers and Heat Pumps*, CRC Press, Cambridge, UK, 2016